Polyhedron 30 (2011) 1219–1224

Contents lists available at ScienceDirect

Polyhedron

journal homepage: www.elsevier.com/locate/poly

Synthesis and characterization of an iron(III) complex of glycine derivative of bis(phenol)amine ligand in relevance to catechol dioxygenase active site

Elham Safaei [a,*], Hamid Sheykhi [a], Andrzej Wojtczak [b], Zvonko Jagličić [c], Anna Kozakiewicz [b]

[a] Institute for Advanced Studies in Basic Sciences (IASBS), 45195 Zanjan, Iran
[b] Nicolaus Copernicus University, Department of Chemistry, 87-100 Torun, Poland
[c] Institute of Mathematics, Physics and Mechanics and Faculty of Civil and Geodetic Engineering, University of Ljubljana, Jadranska 19, SI-1000 Ljubljana, Slovenia

ARTICLE INFO

Article history:
Received 11 November 2010
Accepted 28 January 2011
Available online 17 February 2011

Keywords:
Catechol dioxygenases
Non-heme
Model complex

ABSTRACT

A glycine derivative of bis(phenol)amine ligand (HL^{Gly}) was synthesized and characterized by ^1H NMR and IR spectroscopies. The iron(III) complex ($L^{Gly}Fe$) of this ligand was synthesized and characterized by IR, UV–Vis, X-ray and magnetic susceptibility studies. X-ray analysis reveals that in $L^{Gly}Fe$ the iron(III) center has a distorted trigonal bipyramidal coordination sphere and is surrounded by an amine nitrogen, a carboxylate and two phenolate oxygen atoms. The mentioned carboxylate group acts as μ-bridging ligand for iron centers of neighbor complexes. The variable-temperature magnetic susceptibility indicates that $L^{Gly}Fe$ is the paramagnetic high spin iron(III) complex. It has been shown that electrochemical oxidation of this complex is ligand-centered due to the oxidation of phenolate to the phenoxyl radicals. The $L^{Gly}Fe$ complex also undergoes an electrochemical metal-centered reduction of ferric to ferrous ion. The oxygenation of 3,5-di-*tert*-butyl-catechol, with $L^{Gly}Fe$ in the presence of dioxygen was investigated.

1. Introduction

Mono- and binuclear non-heme iron centers are present in some metalloproteins that perform important biological functions involving dioxygen [1]. The catechol dioxygenases are non-heme iron enzymes that catalyze the oxidative degradation of catechols which are aromatic pollutants. The active site of these enzymes contains iron(III) and amino acid residues such as histidine, tyrosine and glutamic acid [2–10]. These enzymes are divided into two subclasses: the intradiol dioxygenases, catalyzing the cleavage of the carbon–carbon bond between the two catechol oxygen atoms to give muconic anhydride; and the extradiol dioxygenases, which catalyze the cleavage of the carbon–carbon bond adjacent to the catechol oxygen atoms (Scheme 1) giving 2-hydroxymuconic semialdehyde as the product [11].

Tripodal ligands have been used to provide a coordination sphere for synthetic models of enzyme active sites. Iron(III) complexes with N-centered quadridentate tripodal ligands comprising pyridyl [12], carboxylic [13], imidazole [14] moieties, have attracted much attention due to their similarities to the structure and functional of some metalloenzymes including the catechol dioxygenases [3,15–18] purple acid phosphatases [19–21], soybean lipoxygenases [22,23] or galactose oxidase [24]. Several research groups became interested in designing ligands and their iron complexes with phenolate moieties. In the present work, the coordination, magnetic and redox properties of the iron(III) complex $L^{Gly}Fe$ obtained from a glycine derivative of amine bis(phenol) ligand HL^{Gly} are described (Scheme 2).

2. Experimental

2.1. Materials and physical measurements

Reagents or analytical grade materials were obtained from commercial suppliers and used without further purification, except those for electrochemical measurements.

Elemental analyses (C, H, N) were performed by the Research Institute of Petroleum Industry (RIPI). Fourier transform infrared spectroscopy on KBr pellets was performed on a FT-IR Bruker Vector 22 instrument. NMR measurements were performed on a Bruker 250 instrument. UV–Vis absorbance digitized spectra were collected using a Pharmacia Biotech spectrophotometer. The electronic spectra of all complexes were recorded in CH_3OH.

Magnetic susceptibility was measured from powder samples of solid material at the temperature range 2–300 K with a SQUID susceptometer (Quantum Design MPMS-XL-5) in a magnetic field of 1000 Oe.

Voltammetric measurements were performed with a computer controlled Auto Lab electrochemical system (ECO Chemie, Ultrecht, The Netherlands) equipped with a PGSTA 30 model and driven by GPES (ECO Chemie). A glassy carbon electrode with a surface area

* Corresponding author. Tel.: +98 241 4153200; fax: +98 241 4153232.
E-mail address: safaei@iasbs.ac.ir (E. Safaei).

0277-5387/$ - see front matter © 2011 Elsevier Ltd. All rights reserved.
doi:10.1016/j.poly.2011.01.036

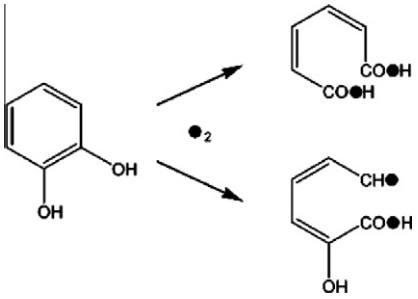

Scheme 1. Scheme of cleavage by intradiol and extradiol dioxygenases [7].

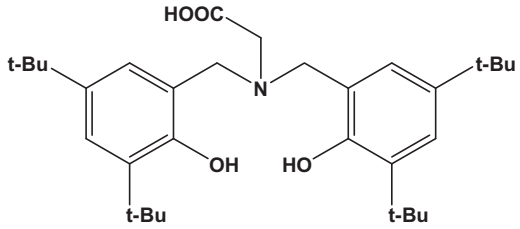

Scheme 2. The structure of bis(phenol)amine HL^{Gly}.

of 0.035 cm^2 was used as a working electrode and a platinum electrode served as the counter electrode. The reference electrode was an Ag wire. Ferrocene was added as an internal standard after completion of a set of experiments, and potentials are referenced vs. the ferrocenium/ferrocene couple (Fc^+/Fc).

The X-ray data for the reported complex FeL^{Gly} were collected with an Oxford Sapphire CCD diffractometer using Mo Kα radiation $\lambda = 0.71073$ Å, at 292(2) K, by $\omega - 2\theta$ method. Structure has been solved by direct methods and refined with the full-matrix least-squares method on F^2 with the use of SHELX97 [25] program package. The numerical absorption correction was applied using RED171 package of programs (Oxford Diffraction, 2000) [26], the maximum and minimum transmission of 0.9492 and 0.8091. Positions of hydrogen atoms have been found from the electron density maps, and hydrogen atoms were constrained during the refinement. The crystallographic data have been deposited with CCDC, the deposition number CCDC 798748.

2.2. Preparations

2.2.1. Synthesis of HL^{Gly}

This ligand was synthesized by the modified literature procedure [27]. A mixture of 2,4-di-*tert*-butylphenol (4.9 g, 24.2 mmol), glycine (0.907 g, 12.1 mmol), and 36% aqueous formaldehyde (4 ml, 48 mmol) was stirred and refluxed for 2 days. The mixture was cooled and filtered and the residue was washed with cold methanol to give the product as a white powder. Further purification was then achieved by washing the precipitate with boiling water and drying the solid in air. The solution remaining after the removal of the solid was left to give more product (5.6 g, 91% yield). *Anal.* Calc. for $C_{32}H_{49}NO_4$ (511.7 g/mol): C, 75.1; H, 8.6; N, 2.7. Found: C, 73.7; H, 9.9; N, 2.6%. ^{1}H NMR ($CDCl_3$-250 MHz): δ 7.27 (s, 2H), 6.93 (s, 2H), 3.85 (s, 4H), 3.49 (s, 2H), 1.53 (s, 18H), 1.14 (s, 18H). ^{13}C NMR($CDCl_3$-250 MHz): 173.97, 152.3, 141.6, 136.5, 125.4, 124.5, 119.56, (77.54, 77.03, 76.53, $CDCl_3$), 57.25, 54.04, 34.86, 34.15, 31.61, 29.70. IR (KBr, cm^{-1}): 3387w, 2958s, 2871sh, 1717s, 1613w, 1476s, 1426sh, 1365s, 1296m, 1227s, 1125s, 1021m, 977m, 874m, 810m, 693m, 654m, 591m. m.p. 122 °C.

2.2.2. Synthesis of $L^{Gly}Fe$

HL^{Gly} (0.511 g, 1 mmol) was added to a solution of triethylamine (0.42 ml, 3 mmol) in methanol (50 ml). The solution was stirred for 10 min at room temperature. Then $Fe(NO_3)_2{\cdot}4H_2O$ (0.404 g, 1 mmol) was added to the solution, the color changed to violet. Subsequently the solution was further stirred at room temperature for 60 min. It was filtered and the solvent was evaporated to give a violet solid, which was subsequently washed with warm water and *n*-hexane. Violet crystals were isolated from a 1:3 mixture of water/acetone. Yield = 0.36 g (63.7%): *Anal.* Calc. for $L^{Gly}Fe$ ($C_{32}H_{46}NO_4Fe$): C, 68; H, 8.2; N, 2.4; Fe, 9.8. Found: C, 64.8; H, 8.5; N, 1.8; Fe, 9.3%. IR (KBr, cm^{-1}): 3420w, 2954s, 2491w, 1627sh, 1576s, 1459s, 1386s, 1284s, 1104m, 1023w, 971m, 916m, 839m, 738m, 611w, 558m, 490m. UV–Vis in CH_2Cl_2: λ_{max}, nm (ε, M^{-1} cm^{-1}): 330 (4980), 474 (3496).

2.2.3. Spectrophotometric investigation of HL^{Gly} and Fe complexation

In an experiment, 2 ml of $FeNO_3{\cdot}4H_2O$ solution in methanol (2.5×10^{-4} M) was transferred into a cuvette. UV–Vis spectra were recorded in the range of 300–800 nm about 5 min after each addition of 10 μL of HL^{Gly} (5×10^{-3} M) solution. Changes in the absorbance of iron nitrate complex upon addition of HL^{Gly} solution were monitored at the maximum of the 540 nm wavelength.

2.2.4. Catalytic oxidation of 3,5-di-tert-butyl-catechol by $L^{Gly}Fe$

$L^{Gly}Fe$ (5% mmol) was added to a solution of triethylamine (2 mmol) in methanol (5 ml) and (1 mmol) 3,5-di-*tert*-butyl-catechol (3,5-DTBC). The solution exposed to dioxygen and stirred for 48 h, the violet color slowly changed to dark green. The progress of the reaction was followed by TLC and ^{1}H NMR spectroscopy. Meanwhile both techniques showed the disappearance of 3,5-DTBC, the products were extracted from the aqueous solution with diethyl ether (3 × 30 ml). The organic layer was separated, washed with 2 M HCl (2 × 20 ml) and then dried over anhydrous Na_2SO_4 at room temperature and then filtered off and the filtrate was evaporated to give 3,5-di-*tert*-butyl-*o*-benzoquinone (3,5-DTBQ) as the major product, and also cleavage products in small amounts. The major product was quantified by comparing the TLC retention factor (Rf) values and ^{1}H NMR signals with the related values of the same sample reported previously [27].

The same experiment was repeated in the absence of any catalyst, no oxidation products were obtained.

3. Results and discussion

Bis-(3,5-di-*tert*-butyl-2-hydroxy-benzyl)-amino-acetic acid HL^{Gly} was synthesized from glycine, formaldehyde, and 2,4-di-*tert*-butyl phenol, in a simple Mannich condensation. Since the formaldehyde used in the reaction contained 63% water, the process was carried in water instead of methanol as reported for similar aminophenol ligands [28].

The ligand HL^{Gly} was treated with iron nitrate, triethylamine in suitable ratio and the solution was refluxed to yield the iron complex $L^{Gly}Fe$ with high yield.

In IR spectra of this complex, the strong and sharp band at 3387 cm^{-1} corresponding to the ν_{OH} stretch of ligand (HL^{Gly}) was replaced by a broad band, proving the coordination of phenol groups to the metal.

Electronic absorption spectra of complexes presented in Section 2.2.2 exhibit intense bands in the near-UV regions (below 300 nm) which are assigned to $\pi \rightarrow \pi^*$ transitions involving the phenolate units. The lowest energy bands (between 450 and 700 nm) are proposed to arise from charge-transfer transitions from the phenolate(π) to Fe(III)($d\pi^*$)[29,30].

3.1. Spectral data analysis of HL^{Gly}–Fe complexation

The titration of ligand (HL^{Gly}) solution at fixed concentration of iron and varying concentration of HL^{Gly} have been conducted. The titration spectra of iron nitrate upon increasing addition of HL^{Gly} are shown in Fig. 1. During the titration, the hypochromicity was observed without any shift in λ_{max} band of 540 nm, which represents the existence of interaction between HL^{Gly} and the iron ion. The appearance of two isosbestic points in iron nitrate spectra clearly indicates the existence of simple equilibrium between HL^{Gly} and HL^{Gly}–Fe. The complex composition of 1:1 was determined by plotting the absorption changes vs. ligand to metal mole ratio ($n_{HL^{Gly}}/n_{Fe}$). Fig. 2 shows a mole ratio plot of iron nitrate upon increasing addition of HL^{Gly}.

3.2. X-ray crystal structure of $L^{Gly}Fe$

The diffraction experiment and the crystal data are summarized in Table 1. The selected bond lengths and angles are given in Table 2.

The asymmetric part of the reported structure consists of the L^{Gly} ligand forming four bonds to the central Fe(III) ion (Fig. 3). The Fe(L^{Gly}) units form the infinite chain along the crystallographic *z*-axis, in which the adjacent Fe centers are bridged by the carboxylic group of the central glycyl moiety of the ligand (Fig. 4). Therefore, each Fe ion has a $FeNO_4$ coordination sphere which has a geometry of a square pyramid deformed towards the trigonal bipyramid (Table 2). The phenolate O1 and O2 form short bonds to the Fe(III), the distances being 1.859(5) and 1.824(5) Å, respectively. The carboxylate O3 participates in the Fe1–O3 bond of 2.020(5) Å, while the O4 atom forms the 1.985(5) Å bond to the adjacent Fe1 [$x, -y-1, z-1/2$]. A series of such bonds formed by the carboxylate groups leads to the formation of the one-dimensional chain of Fe(L^{Gly}) units. The longest bond within the coordination sphere is formed by N1 atom, with the Fe–N distance of 2.207(5) Å. The steric demands for the pentadentate coordination of L^{Gly} result in the elongation of the Fe–N1 bond and the wide range of the bond angles found in the coordination sphere. The angles between the bonds formed by O1, O2 and O3 are in a range 110.4(2)–134.1(2)°. The O–Fe–N1 angles involving these O atoms vary from O3–Fe1–N1 76.80(19)° to O2–Fe1–N1 92.4(2)°. The angles between bonds involving O1, O2 or O3 and the Fe1–O4 [$x, -y-1, z+1/2$] are also close to 90° (from 81.06(19)° to 108.7(2)°). The O4 [$x, -y-1, z+1/2$] and N1 atoms are positioned axially, with the N–Fe–O angle being 153.7(2)°. The Fe(III) complexes containing L^{Gly} or its analogs with different substituents replacing ^{t}Bu groups and additional N_2-type ligand have been reported before [31,32]. For these complexes, the similar bond lengths were reported within the coordination sphere. However, only in the Fe(L^{Gly}) complex reported here the coordination sphere is so deformed and the carboxylate group participates in the bridging interactions between adjacent Fe centers.

The valence geometry of the L^{Gly} ligand is typical for such molecules. Conformation of the central C1–C6–C7–N1–C8–C9–C14 fragment is described with the consecutive torsion angles of 61.7(8)°, −171.5(6)°, 61.4(7)° and 62.2(8)°. The dihedral angle between the phenolate rings of the same ligand is 61.5(3)°, while the angles between the C1–C6 and C9–C14 rings and the five-membered Fe1–O3–C32–C31–N1 chelate ring are 84.6° and 33.9°, respectively. Such a geometry results in the quasi-helical arrangement of the central C_3–N–C_3 chain and phenolate rings along the infinite Fe(L^{Gly}) chain (Fig. 5). That arrangement is the reason for the non-centrosymmetric space group determined for the investigated compound.

Table 1
Crystal data and structure refinement for $L^{Gly}Fe$.

Identification code	$L^{Gly}Fe$
Empirical formula	$C_{32}H_{46}FeNO_4$
Formula weight	564.55
Temperature (K)	292(2)
Wavelength (Å)	0.71073
Crystal system, space group	orthorhombic, *Iba*2
Unit cell dimensions	
a (Å)	33.9445(17)
b (Å)	20.0897(8)
c (Å)	9.2855(4)
Volume (Å^3)	6332.1(5)
Z, D_{calc} (mg/m^3)	8, 1.184
Absorption coefficient (mm^{-1})	0.510
F(0 0 0)	2424
Crystal size (mm)	0.43 × 0.14 × 0.10
θ Range for data collection (°)	2.36–26.00
Limiting indices	$-41 \le h \le 41$ $-24 \le k \le 23$ $-11 \le l \le 8$
Reflections collected/unique	21621/5203 [R_{int} = 0.1413]
Completeness to θ = 26.00	99.8%
Absorption correction	Numerical
Maximum and minimum transmission	0.9492 and 0.8091
Refinement method	Full-matrix least-squares on F^2
Data/restraints/parameters	5203/7/343
Goodness-of-fit on F^2	1.021
Final *R* indices [$I > 2\sigma(I)$]	R_1 = 0.0712, wR_2 = 0.1541
R indices (all data)	R_1 = 0.1319, wR_2 = 0.1773
Absolute structure parameter	0.05(4)
Largest differences in peak and hole (e Å^{-3})	0.523 and −0.828

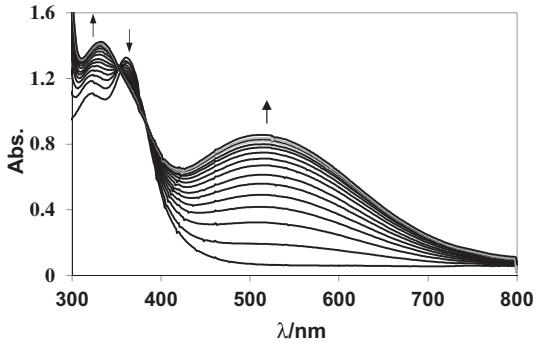

Fig. 1. The titration absorption spectra of $Fe(NO_3)_3$ (2.5×10^{-4} M) by HL^{Gly} (2.5×10^{-5}, 5×10^{-5}, 7.5×10^{-5}, 1×10^{-4}, 1.25×10^{-4}, 1.5×10^{-4}, 1.75×10^{-4}, 2×10^{-4}, 2.25×10^{-4}, 2.5×10^{-4}, 2.75×10^{-4}, 3×10^{-4}, 3.25×10^{-4}, 3.5×10^{-4}, 3.75×10^{-4}, 4×10^{-4}, 4.25×10^{-4}, 4.5×10^{-4} M).

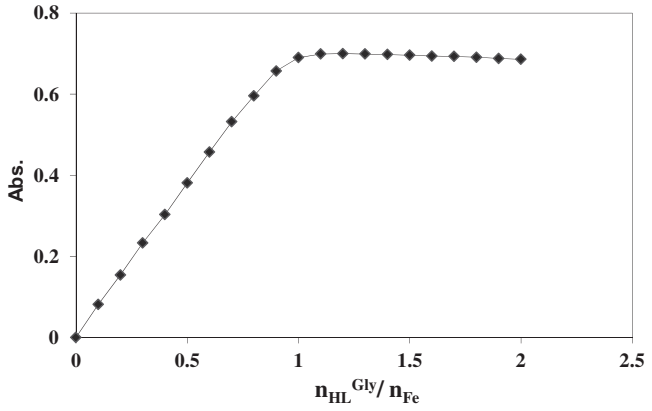

Fig. 2. Determination of complex composition by the mole ratio plot.

Table 2
Selected bond lengths [Å] and angles [°] for $L^{Gly}Fe$.

Fe1–O2	1.824(5)
Fe1–O1	1.859(5)
Fe1–O4#1	1.985(5)
Fe1–O3	2.020(5)
Fe1–N1	2.207(5)
O1–C1	1.343(8)
C6–C7	1.489(10)
C7–N1	1.488(8)
N1–C31	1.461(9)
N1–C8	1.484(8)
C8–C9	1.476(9)
C14–O2	1.353(8)
C31–C32	1.477(9)
C32–O4	1.258(8)
C32–O3	1.259(8)
O4–Fe1#2	1.986(5)
O2–Fe1–O1	113.6(2)
O2–Fe1–O4#1	108.7(2)
O1–Fe1–O4#1	96.6(2)
O2–Fe1–O3	110.4(2)
O1–Fe1–O3	134.1(2)
O4#1–Fe1–O3	81.06(19)
O2–Fe1–N1	92.4(2)
O1–Fe1–N1	88.8(2)
O4#1–Fe1–N1	153.7(2)
O3–Fe1–N1	76.80(19)
C1–O1–Fe1	129.2(4)
O1–C1–C6	118.7(7)
O1–C1–C2	121.0(6)
C5–C6–C7	121.1(7)
C1–C6–C7	119.5(7)
N1–C7–C6	113.5(5)
C31–N1–C8	109.4(5)
C31–N1–C7	111.9(5)
C8–N1–C7	110.5(5)
C31–N1–Fe1	106.8(4)
C8–N1–Fe1	105.9(4)
C7–N1–Fe1	112.1(4)
C9–C8–N1	116.1(6)
O2–C14–C9	118.6(6)
O2–C14–C13	121.4(6)
C9–C14–C13	119.9(7)
C14–O2–Fe1	128.8(4)
N1–C31–C32	110.4(6)
O4–C32–O3	124.2(6)
O4–C32–C31	117.8(6)
O3–C32–C31	118.0(6)
C32–O3–Fe1	119.4(4)
C32–O4–Fe1#2	137.7(4)

Symmetry transformations used to generate equivalent atoms: #1 $x, -y-1, z+1/2$; #2 $x, -y-1, z-1/2$.

The six-membered chelate rings Fe1–N1–C7–C6–C1–O1 and Fe1–N1–C8–C9–C14–O2 have a boat conformation, while the five-membered Fe1–O3–C32–C31–N1 ring is an envelope on N1.

Analysis of the non-bonding interactions in the reported structure revealed four intramolecular interactions involving C17, C18, C28 and C29 C–H groups of ^{t}Bu and phenolate O1 or O2, with the C···O distances varying from 3.0323 to 3.141 Å. Also the C–H···π interaction between C17–H17B and the ring C1–C6 is found, the distance between H17B and the center of gravity (Cg) of the ring being H···Cg [x, $1-y$, $1/2+z$] 2.96 Å.

3.3. Magnetic susceptibility measurements

Magnetic susceptibility for powdered samples of $L^{Gly}Fe$ was measured in a magnetic field of 1000 Oe as a function of temperature in the range 2–300 K. The measured data were corrected for the temperature-independent Larmor diamagnetic susceptibility obtained from the Pascal's tables [33] and for the sample holder contribution. The magnetic diagram is presented in Fig. 6 in the form of μ_{eff} vs. T.

Above $T \approx 15$ K, the effective magnetic moment (μ_{eff}) of complex $L^{Gly}Fe$ is essentially temperature-independent and has μ_{eff} value of 5.45 μ_B, what is in a good agreement with the expected value (5.92 μ_B) for the isolated $S = 5/2$ Fe(III) ion. Thus the magnetic measurement of this complex shows unambiguously that $L^{Gly}Fe$ contains the magnetically diluted high-spin d^5 iron(III) ion.

Below 15 K, the effective magnetic moment (μ_{eff}) slightly decreases and the Curie–Weiss fit of the high temperature data (above 100 K) gave $\theta = -0.8$ K. Decrease of the effective magnetic moment and a small negative value of Curie–Weiss temperature θ might be due to a zero field splitting or(and) a weak antiferromagnetic interaction between adjacent Fe(III). In the latter case from the mean field theory [34], we have estimated the exchange integral $J/k_B = 3\theta/(2zS(S+1)) = -0.07$ K (or -0.05 cm^{-1}), where we used $z = 2$ nearest neighbours and $S = 5/2$.

3.4. Electrochemistry

Cyclic voltammograms (CV) of $L^{Gly}Fe$ (3×10^{-3} M) have been recorded in CH_3CN solutions containing 0.1 M $LiClO_4$ as a supporting electrolyte at −40 °C (Fig. 7). Prior to the measurement, the GC electrode was polished with 0.1 mm alumina powder and washed with distilled water. The voltage scan rate was set at 50 mV s^{-1}. The solutions were deoxygenated by bubbling the nitrogen gas through them. Ferrocene was added as an internal standard after

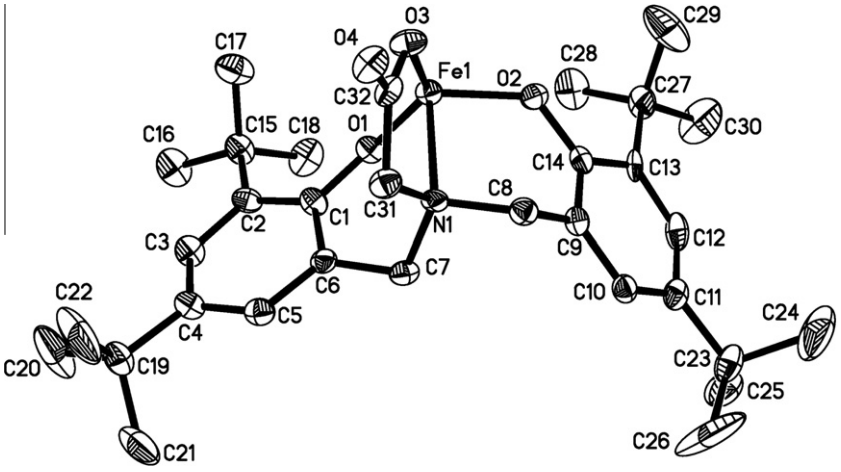

Fig. 3. ORTEP diagram and atom labeling scheme for the asymmetric unit of complex $L^{Gly}Fe$. Ellipsoids are plotted at 30% probability level. Hydrogen atoms omitted for clarity.

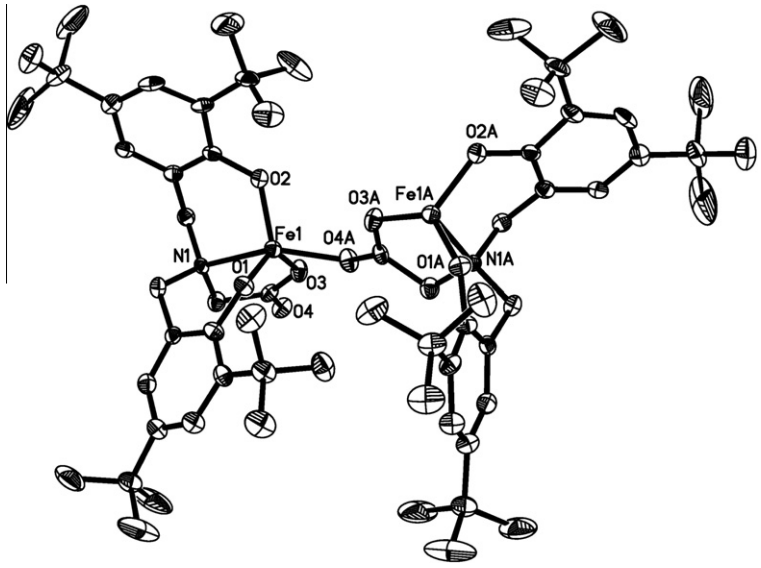

Fig. 4. The details of the interactions between the adjacent $L^{Gly}Fe$ complex molecules leading to the formation of the chain supramolecular structure.

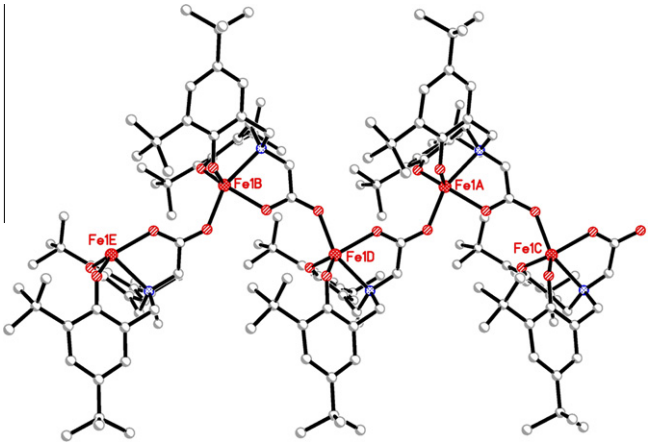

Fig. 5. The chain structure of $L^{Gly}Fe$. For clarity, the hydrogen atoms are omitted.

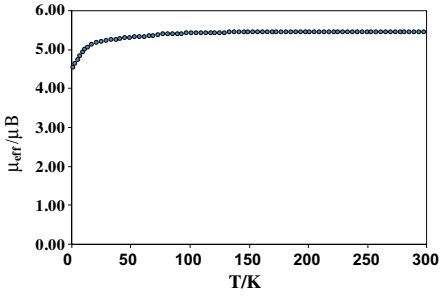

Fig. 6. Magnetic measurements for complex $L^{Gly}Fe$.

completion of a set of experiments, and potentials are referenced vs. the ferrocenium/ferrocene couple (Fc^+/Fc).

The CV voltammograms observed with $L^{Gly}Fe$ exhibit the irreversible oxidation (E_1^{ox}) and reduction peaks at 0.18 V and −1.1 V, respectively. The oxidation process was probably attributed to the ligand-centered oxidation yielding the phenoxyl radical in the complex, but there is no direct evidence available yet. The metal-centered voltammograms, which have been observed at the

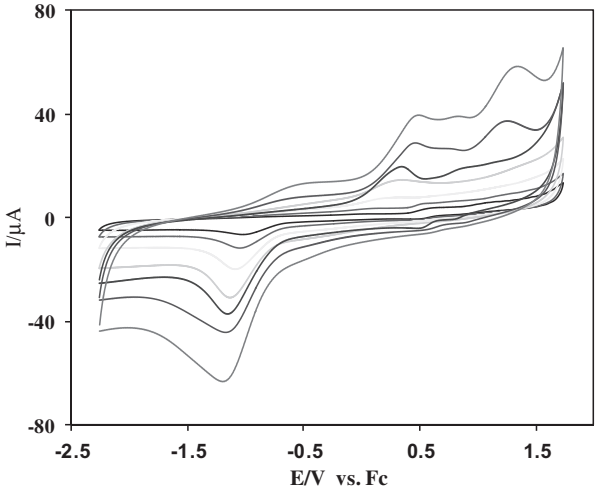

Fig. 7. Cyclic voltammetry of $L^{Gly}Fe$ (3×10^{-3} M) in CH_3CN with M $LiClO_4$ as supporting electrolyte. Potentials are referenced vs. Fc, Scan rate is 50 mV/s and $T = -40$ °C.

negative potential range, reveal the Fe^{III}/Fe^{II} reduction of $L^{Gly}Fe$. They are chemically irreversible, what suggests the instability of the oxidized and reduced species.

3.5. $L^{Gly}Fe$-catalyzed oxidation of 3,5-di-tert-butyl-catechol

The focus of this experimental part was to catalyze the oxygenation of catechols, with dioxygen as an oxidant. In the presence of 5% of the catalyst, 100% of 3,5-di-*tert*-butyl-catechol (3,5-DTBC) was converted to 3,5-di-*tert*-butyl-*o*-benzoquinone (3,5-DTBQ) as the major product, and also cleavage products in small amounts (Scheme 3). Progress of the reaction was followed by ^1H NMR spectroscopy. The signals of the free substrate (δ 6.90, 1.37, 1.23) disappeared along with the appearance of signals of the 3,5-DTBQ (δ 6.93, 6.22, 1.28, 1.23) [35,36]. The results show that the $L^{Gly}Fe$ complex can act as a good catalyst of the 3,5-DTBC oxidation to 3,5-DTBQ in a presence of oxygen. The ^1H NMR shows the 100% conversion of 3,5-DTBC producing 69.9% benzoquinone, 17.9% of a

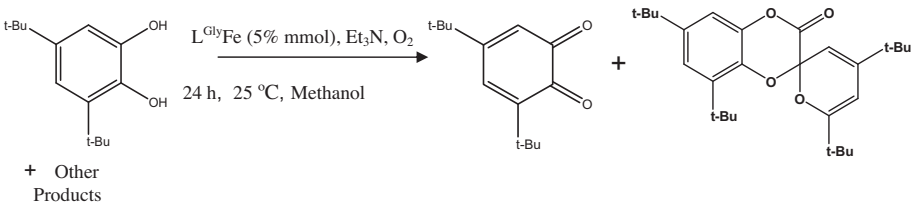

Scheme 3. Oxidation of 3,5-DTBC by $L^{Gly}Fe$.

cleavage product (Scheme 3) and 12.2% of a mixture of unknown products (Figs. 1S–3S).

4. Conclusion

The ligand bis-(3,5-di-*tert*-butyl-2-hydroxy-benzyl)-amino-acetic acid, HL^{Gly} was prepared by a simple green synthesis. The two phenolate moieties, one carboxylate group and the central tertiary amine in HL^{Gly} provide a NO_3 donor set. The iron(III) complex of this tripodal tetradentate ligand. Was synthesized and characterized.

X-ray analysis reveals that $L^{Gly}Fe$ crystallizes in the orthorhombic crystal system. It has a distorted trigonal bipyramid geometry in which the iron(III) center has been surrounded by an amine nitrogen, a carboxylate and two phenolate oxygen atoms. The carboxylate group acts as μ-bridging ligand for iron centers of neighbor complexes leading to the formation of the infinite chains of the $L^{Gly}Fe$ units.

The variable-temperature magnetic susceptibility indicates that $L^{Gly}Fe$ is the paramagnetic high spin iron(III) complex in almost whole investigated temperature range. Only below 15 K the effective magnetic moment slightly decreases which may be due to a zero field splitting or a very week antiferromagnetic interaction between iron(III) ions effective only at low temperature.

Redox process of $L^{Gly}Fe^{III}$ yielded the corresponding Fe(III)-phenoxyl radical and $L^{Gly}Fe^{II}$ species during the cyclic voltammetry experiments.

The catalytic experiments show that $L^{Gly}Fe$ complex can act as a good catalyst for the oxidation (and not the oxidative cleavage) of 3,5-DTBC to 3,5-DTBQ in a presence of oxygen.

Acknowledgments

Authors are grateful to the Institute for Advanced Studies in Basic Sciences (IASBS), Nicolaus Copernicus University and University of Ljubljana, for their valuable help. E. Safaei gratefully acknowledges the support by the Institute for Advanced Studies in Basic Sciences (IASBS) Research Council under Grant No. G2011IASBS127.

Appendix A. Supplementary data

CCDC 798748 contains the supplementary crystallographic data for $L^{Gly}Fe$. These data can be obtained free of charge via http://www.ccdc.cam.ac.uk/conts/retrieving.html, or from the Cambridge Crystallographic Data Centre, 12 Union Road, Cambridge CB2 1EZ, UK; fax: (+44) 1223-336-033; or e-mail: deposit@ccdc.cam.ac.uk.

References

[1] J.D. Lipscomb, A.M. Orville, in: H. Sigel, A. Sigel (Eds.), Metal Ions in Biological Systems, vol. 28, New York, 1992, pp. 243–298.
[2] T.D.H. Bugg, C.J. Winfield, Nat. Prod. Rep. 15 (1998) 513.
[3] D.H. Ohlendorf, J.D. Lipscomb, P.C. Weber, Nature 336 (1988) 403.
[4] S. Han, L.P. Eltis, K.N. Timmis, S.W. Muchmore, J.T. Bolin, Science 270 (1996) 976.
[5] K. Sugimoto, T. Senda, H. Aoshima, E. Masai, M. Fukuda, Y. Mitsui, Structure 7 (1999) 953.
[6] H.G. Jang, D.D. Cox, L. Que Jr., J. Am. Chem. Soc. 113 (1991) 9200.
[7] T. Kojima, R.A. Leising, S. Yan, L. Que Jr., J. Am. Chem. Soc. 115 (1993) 11328.
[8] H. Zheng, L. Que Jr., Inorg. Chim. Acta 263 (1997) 301.
[9] R. Viswanathan, M. Palaniandavar, T. Balasubramanian, T.P. Muthiah, Inorg. Chem. 37 (1998) 2943.
[10] M.P. Jensen, S.J. Lange, M.P. Mehn, E.L. Que, L. Que Jr., J. Am. Chem. Soc. 125 (2003) 2113.
[11] L. Que, R.Y.N. Ho, Chem. Rev. 96 (1996) 2607.
[12] J. Hwang, K. Govindaswamy, S.A. Koch, Chem. Commun. (1998) 1667.
[13] L. Que Jr., R.C. Kolanczyk, L.S. White, J. Am. Chem. Soc. 109 (1987) 5373.
[14] L.E. Cheruzel, J. Wang, M.S. Mashuta, R.M. Buchanan, Chem. Commun. (2002) 2166.
[15] L. Que Jr., R.Y.N. Ho, Chem. Rev. 96 (1996) 2607.
[16] D.H. Ohlendorf, A.M. Orville, J.D. Lipscomb, J. Mol. Biol. 244 (1994) 586.
[17] S. Han, L.D. Eltis, K.N. Timmis, S.W. Muchmore, J.T. Bolin, Science 270 (1995) 976.
[18] T. Senda, K. Sugiyama, H. Narita, T. Yamamoto, K. Kimbara, M. Fukuda, M. Sato, K. Yano, Y. Mitsui, J. Mol. Biol. 255 (1996) 735.
[19] B.C. Antanaitis, T. Strakas, P. Aisen, J. Biol. Chem. 257 (1982) 3766.
[20] J.C. Davis, B.A. Averill, Proc. Natl. Acad. Sci. USA 79 (1982) 4623.
[21] B.C. Antanaitis, P. Aisen, Adv. Inorg. Biochem. 5 (1983) 111.
[22] J.C. Boyington, B.J. Gaffney, M. Arnzel, Science 260 (1993) 1482.
[23] W. Minor, J. Steczko, J.T. Bolin, Z. Otwinowski, B Axelrod, Biochemistry 32 (1993) 6320.
[24] N. Ito, S.E.V. Phillips, K.D.S. Yadav, P.F. Knowles, J. Mol. Biol. 238 (1994) 794.
[25] G.M. Sheldrick, SHELXS97 and SHELXL97, University of Göttingen, Germany, 1997.
[26] CRYSALIS CCD171 and RED171 package of programs, Oxford Diffraction, 2000.
[27] V.I. Lodyato, I.L. Yurkova, V.L. Sorokin, O.I. Shadyro, V.I. Dolgopalets, M.A. Kisel, Bioorg. Med. Chem. Lett. 13 (2003) 1179.
[28] E.Y. Tshuva, I. Goldberg, M. Kol, Organometallics 20 (2001) 3017.
[29] E.J. Land, G. Porter, Trans. Faraday Soc. 59 (1963) 2016.
[30] L.I. Grossweiner, W.A. Mulac, Rad. Res. 10 (1959) 515.
[31] M. Roy, S. Saha, A.K. Patra, M. Nethaji, A.R. Chakravarty, Inorg. Chem. 46 (2007) 4368.
[32] M.S. Shongwe, C.H. Kaschula, M.S. Adsetts, E.W. Ainscough, A.M. Brodie, M.J. Morris, Inorg. Chem. 44 (2005) 3070.
[33] L. Dutta, A. Syamal, Elements of Magnetochemistry, Affiliated East-West Press Pvt. Ltd., 1993. pp. 6–11.
[34] C. Kittel, Introduction to Solid State Physics, eighth ed., John Wiley and Sons, 2005.
[35] C. Limberg, M. Wagner, T. Tietz, Chem. Eur. J. 15 (2009) 5567.
[36] R.G. Finke, H. Weiner, J. Am. Chem. Soc. 121 (1999) 9831.